OPEN ACCESS
IOP Publishing
Journal of Physics A: Mathematical and Theoretical
J. Phys. A: Math. Theor. **54** (2021) 345203 (16pp)
https://doi.org/10.1088/1751-8121/ac16c4

Honeycomb structures in magnetic fields

Becker Simon[1,*], Rui Han[2], Svetlana Jitomirskaya[3] and Maciej Zworski[4]

[1] Department of Applied Mathematics and Theoretical Physics, University of Cambridge, Wilberforce Road, Cambridge, CB3 0WA, United Kingdom
[2] School of Mathematics, Louisiana State University, Baton Rouge, Louisiana, 70803, United States of America
[3] Department of Mathematics, University of California, Irvine, CA 92697, United States of America
[4] Department of Mathematics, University of California, Berkeley, CA 94720, United States of America

E-mail: slb214@cam.ac.uk

Received 31 March 2021, revised 23 June 2021
Accepted for publication 21 July 2021
Published 5 August 2021

Abstract

We consider the nearest-neighbour tight binding model of the honeycomb lattice in magnetic fields and discover surprizing new analytical results that fully explain fractal spectra and experimentally observed asymmetries in the density of states of molecular graphene. We describe a fractal Cantor spectrum for irrational magnetic flux through a honeycomb, and establish the existence of zero energy Dirac cones for each rational flux with fully explicit estimates on the cone angle. Our results give a substantially more refined description of subtleties in the de Haas–van Alphen and quantum Hall effects, and provide the first quantitative bounds on transport coefficients for the tight-binding model under disorder.

Keywords: honeycomb, magnetic, Cantor spectrum, Anderson model, semiclassical analysis, quantum Hall effect, de Haas van Alphen effect

(Some figures may appear in colour only in the online journal)

The tight binding model on the honeycomb lattice is of central importance in condensed matter physics as it is analytically tractable and describes qualitative material properties fairly

*Author to whom any correspondence should be addressed.

accurately. In this article, we consider the nearest-neighbour tight-binding model of the honeycomb lattice with an additional constant magnetic field, perpendicular to the lattice and derive several new properties for this model.

Expansions of the density of states (DOS) for perfect Dirac cones have been obtained for example in [1, (42)] and [2, (4.2)]. From the DOS, one can then derive magnetic oscillations, going back to Onsager [3], studied for graphene in [2, 4, 5] in which the famous *sawtooth* pattern of the magnetization has already been observed. This analysis has been refined in [9] by taking the additional *Harper broadening* of the Landau levels into account, i.e. spectral effects that are not captured by the simplified expansion into Landau levels directly. In practice, the Dirac cones are not perfect cones [10, 11] and perturbations from this idealized conical structure have to be taken into account. In this article, we derive such refined asymptotic for magnetic oscillations under the assumption of a constant chemical potential. This assumption on the chemical potential is also present in the 3D Lifshitz–Kosevich theory [12] for the study of magnetic oscillations in the susceptibility of metals at low temperatures. A 2D analogue of the theory for metals has been developed by Shoenberg [13] and was discussed in the context of graphene in [5]. Further connections between the DOS and oscillations in electric and also thermal conductivities have for example been considered in [14, 15], where usually the assumption of perfect Landau levels is made. An experimental observation of the Shubnikov–de Haas oscillation in graphene has been achieved in [16]. In this article, we treat the case of slightly asymmetric Dirac cones and extend the above results by providing an expansion of the DOS that is valid near any rational magnetic flux. The asymmetry of the Dirac cones explains an asymmetry that has been observed in molecular graphene [17], see also explanations based on higher interactions [18] and experimental verifications thereof [19]. While there is no such asymmetry for the tight-binding model due to particle–hole symmetry, the quantum graph model for graphene does not have this symmetry. We then extend our results for small magnetic fields to magnetic fields close to any rational flux, show that the Dirac cones are topologically protected in the tight-binding model, see also [20], where it is argued that there are Dirac points due to chiral symmetry, and explicitly compute their Fermi velocity. Our new theoretical insights could be of key importance in quantitatively explaining magnetic minibands and experimentally observing the de Haas–van Alphen effect in graphene.

While the DOS of the tight-binding model of graphene has been extensively investigated before, much less is known about the nature of the spectrum of the tight-binding model in a constant magnetic field, apart from regimes of low-lying spectrum [21]. The fractal structure of magnetic electron spectra was first predicted by Azbel [22] and then numerically confirmed by Hofstadter [23] for Harper's model. Verifying this experimentally is difficult as the smallness of the cell requires extraordinarily strong magnetic fields to obtain observable magnetic flux. Only recently, self-similar structures in the electron spectrum of graphene have been observed [7, 8, 24, 25]. Earlier experiments involved modelling of periodic structures by microwaves [26].

Following a thorough mathematical study of tight-binding models over the past fourty years, rigorous results on the fractal spectrum on the $\mathbb{Z}^2$-lattice (*Harper's model*) [27–36] and the location of the low-lying spectrum [37–40] have been obtained. This included a heuristic and computational analysis of the fractal dimension of the spectrum [41–43]. By a conjecture that is often attributed to Wilkinson and Austin [44], the fractal dimension of the tight-binding model is $1/2$. We show that for irrational magnetic flux, the spectrum is a nowhere dense without isolated points and the Hausdorff dimension can indeed not exceed $1/2$.

In the last part of the article, we then study also the magnetic tight-binding model with Anderson-type disorder [45, 47, 48] close to arbitrary rational magnetic flux. We study transport properties and the quantum Hall effect. [46]

To summarize, the purpose of this article is to report, for the first time, on a variety of tight-binding and quantum graph models for honeycomb structures in constant magnetic fields and emphasize new theoretical approaches that potentially apply to more general systems.

To be more precise, in this article, we discuss progress on three key physical phenomena:

- *Spectral theoretic*: we provide a comprehensive and highly elaborate spectral analysis. In particular, we show that for irrational magnetic flux through a single honeycomb, the spectrum is a Cantor set of measure zero and the Hausdorff dimension of the spectrum is at most $1/2$ [49, 50].
- *Semiclassical*: we derive a semiclassical expansion for the DOS, with error bounds, supported on geometric Landau levels and relate it to the Shubnikov–de Haas, de Haas–van Alphen, and quantum Hall effects [10, 51]. In addition, we provide a solid foundation to experimentally observed asymmetries of the DOS in molecular graphene [17]. Figure 5 illustrates a remarkable agreement of our asymptotic expansion for the magnetization with exact spectral calculations. Our analysis applies to all conical singularity, which we show to exist for each rational magnetic flux. This result also provides a foundation for self-similarity appearing in the Hofstadter butterfly on the hexagonal lattice which can be easily seen in the Hofstadter butterfly for the honeycomb lattice depicted in figure 6.
- *Dynamical*: for Anderson-type potentials in weak magnetic fields under weak disorder, we identify insulating regions away from the Landau levels in which Anderson localization occurs, and regions of metallic transport close to the Landau levels [51]. In particular, our results yield, for the first time, quantitative estimates on the transport coefficients for the honeycomb lattice.

We start by introducing the quantum graph model and explain how it relates to the standard tight-binding model on the honeycomb lattice. As a rule, we shall set all physical constants equal to one in this article. The Hamiltonian, H^B, of the quantum graph with constant magnetic field B, defined on edges e, that we can identify, as they are just straight lines, with intervals $(0, 1)$, of a honeycomb graph Λ is defined as

$$H_e^B := (-i\partial_x - A_e)^2 + V_e, \quad e \simeq (0, 1). \tag{1}$$

We assume Kirchhoff boundary conditions [52] for the wavefunction $\psi = (\psi_e)_e$ at the vertices v of the graph associated to the honeycomb lattice. This means, that for all edges e adjacent to a vertex v of the graph

$$\sum_{e;v \text{ belongs to } e} \psi_e'(v) = 0.$$

In addition, we assume that the potential $V = (V_e)$ of the Hamiltonian has the property that V_e is symmetric with respect to the centre of the edge and independent of the edge e. Such Hamiltonians are called *quantum graphs* or *wave guides* [6, 52] and represent the infinite-contrast limits [53] of continuous Schrödinger operators on $\mathbb{R}^2$ with honeycomb lattice potential [54–57]. Apart from the interest in such models as limits (see [58, 59] for related work on Harper's model), quantum graphs are natural models for *molecular graphene* [17, 60] and *wave guides* [26]. To define the Hamiltonian (1) it remains to define the magnetic vector potentials A_e. In fact, for vector potentials $A(x) = (A_1(x), A_2(x))$, the scalar potential A_e entering in (1) along edges e is, as has been explained in [6], given by

$$A_e(x) := A(x) \cdot \vec{e},$$

where $\vec{e}$ is the direction of the edge and $\cdot$ denotes the inner product of vectors. The magnetic flux $h := \int_{\hexagon} \mathrm{d}A$ through each honeycomb $\hexagon$ of the lattice is taken to be constant. Our choice of the variable h, to denote the magnetic flux, is motivated by our semiclassical analysis for small magnetic fluxes where h is the standard notation for the semiclassical parameter. It is well-known that the Hamiltonian H^B, defined in (1) which is a differential operator on the honeycomb graph can be identified with the standard magnetic tight-binding operator t^h on the discrete honeycomb lattice. This result can for example be found in [49, 59, 61–63]. To elaborate on this point, recall that as for example shown in [64] a simple change of geometry, the nearest-neighbour magnetic tight-binding operator t^h is given as

$$t^h = \frac{1}{3}\begin{pmatrix} 0 & 1+\tau^0+\tau^1 \\ \left(1+\tau^0+\tau^1\right)^\dagger & 0 \end{pmatrix} \quad \text{on } \mathbb{Z}^2, \tag{2}$$

where in the above operator, we use discrete magnetic translations, acting on vertices r of the honeycomb lattices

$$\tau^0(r)(\gamma) := r(\gamma_1 - 1, \gamma_2), \quad \tau^1(r)(\gamma) := \mathrm{e}^{\mathrm{i}h\gamma_1}\, r(\gamma_1, \gamma_2 - 1)$$

for $\gamma \in \mathbb{Z}^2$, and $r \in \ell^2(\mathbb{Z}^2;\mathbb{C})$ is a square-summable sequence. Here $\ell^2(\mathbb{Z}^2;\mathbb{C})$ is the space of square-summable sequences on $\mathbb{Z}^2$. The connection between operators (1) and (2) is then as follows: if we solve the differential equation

$$-y_\lambda''(x) + V_e y_\lambda(x) = \lambda y_\lambda(x),$$

with initial conditions $y_\lambda(0) = 1$ and $y_\lambda'(0) = 0$, we can uniquely define the so-called Floquet discriminant $\Delta(\lambda) := y_\lambda(1)$. The Floquet discriminant oscillates, as a function of λ between values $\geqslant 1$ and values $\leqslant -1$.

We then define the Dirichlet operator with eigenvalues λ and eigenfunctions ψ on $(0,1)$ such that

$$H^{\mathrm{D}}_{(0,1)}\psi = -\psi'' + V_{(0,1)}\psi = \lambda\psi,$$

where ψ satisfies Dirichlet boundary conditions $\psi(0) = \psi(1) = 0$ and $V_{(0,1)}$ is the same potential as the one in (1).

Then, we have the following equivalence relation between spectra:

$$\lambda \in \mathrm{Spec}(H^B)\backslash\mathrm{Spec}(H^D) \text{ if and only if } \Delta(\lambda) \in \mathrm{Spec}(t^h),$$

where Spec denotes the spectrum of the operator. In this sense, the quantum graph Hamiltonian (1) and the tight-binding model (2) are equivalent up to some discrete set, $\mathrm{Spec}(H^D)$, the spectrum of the Hamiltonian with Dirichlet boundary conditions. Since the operator norm of the tight-binding operator (2) satisfies $\left\|t^h\right\| < 1$ [49, 59] for non-trivial magnetic flux $h \notin 2\pi\mathbb{Z}$, the spectrum of the tight-binding model (2) is strictly contained in the interval $(-1, 1)$. Due to this, the spectrum of the quantum graph Hamiltonian H^B, given in (1), decomposes into the disjoint union of continuous spectrum $\Delta^{-1}(\mathrm{Spec}(t^h))$, that is fully determined by the tight-binding Hamiltonian t^h, and infinitely degenerate eigenvalues $\lambda \in \mathrm{Spec}(H^D)$, see [49].

This is precisely because the Dirichlet spectrum of H^D is located at energies $\lambda \in \Delta^{-1}(\pm 1)$.

1. Cantor spectrum

To understand the spectrum of the Hamiltonian for irrational magnetic flux $\frac{h}{2\pi}$, we approximate the irrational value of the flux by rational ones. Therefore, we first assume that the normalized

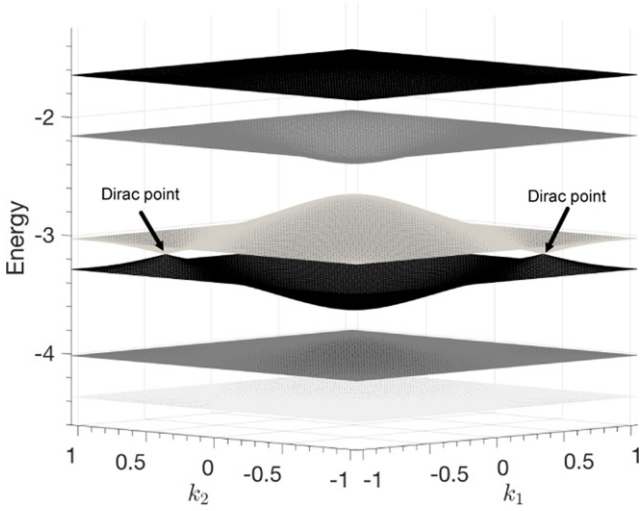

Figure 1. We show that Dirac points persist under rational flux $\frac{h}{2\pi} \in \mathbb{Q}$. Here, we plot the Floquet bands for a rational magnetic flux $\frac{h}{2\pi} = \frac{1}{3}$ with Mathieu potential $V(x) = 20\cos(2\pi x)$, that we choose for illustrative purposes as it is explicitly solvable, for the quantum graph Hamiltonian (1).

magnetic flux $\frac{h}{2\pi} = \frac{p}{q}$ is rational, as then the Floquet–Bloch theory implies that the spectrum of (2) has band structure. This is illustrated in figure 1 where bands of the tight-binding operator are plotted for a magnetic flux $\frac{h}{2\pi} = \frac{1}{3}$. This means that the spectrum consists of a finite union of disjoint intervals. We now return to the study of irrational $\frac{h}{2\pi}$: by approximating the irrational flux by suitable rational ones, we first use the supersymmetry, i.e. off-diagonal matrix structure, of (2) and then a one-dimensional Floquet transform in the periodic direction, to reduce the study of the spectrum of (2) to that of a one-dimensional Jacobi operator with quasi-momentum $k \in \mathbb{T}_1^* = [0, 2\pi]$ and $m \in \mathbb{Z}$

$$(J_k u)_m = \left(1 + \mathrm{e}^{\mathrm{i}(k+mh)}\right) u_{m+1} + 2\cos(k + mh)\, u_m + \left(1 + \mathrm{e}^{\mathrm{i}(k+(m-1)h)}\right) u_{m-1}. \tag{3}$$

Thus, we can express the spectrum of the tight-binding operator (2) as

$$\mathrm{Spec}(t^h) = \bigcup_{k\in[0,2\pi]} \mathrm{Spec}(J_k). \tag{4}$$

We shall now show that the spectrum is fractal, i.e. a Cantor set for $\frac{h}{2\pi}$ being irrational. By this we mean a nowhere dense set without isolated point. In order to do so, it suffices to show that the measure of the spectrum is zero. This is because isolated points in the spectrum would imply the existence of point spectrum which can be excluded by general principles. Hence, since the spectrum of closed, the Cantor-structure follows once we establish that its Lebesgue measure is zero (figure 2).

To do so, we can use a quite general analysis of Jacobi operators that we establish in [49, lemma 4.3], by which we can then estimate the Lebesgue measure of the spectrum of the tight-binding operator, using (4). This implies, that for some $C > 0$ and flux h satisfying $\frac{h}{2\pi} = \frac{p}{q}$,

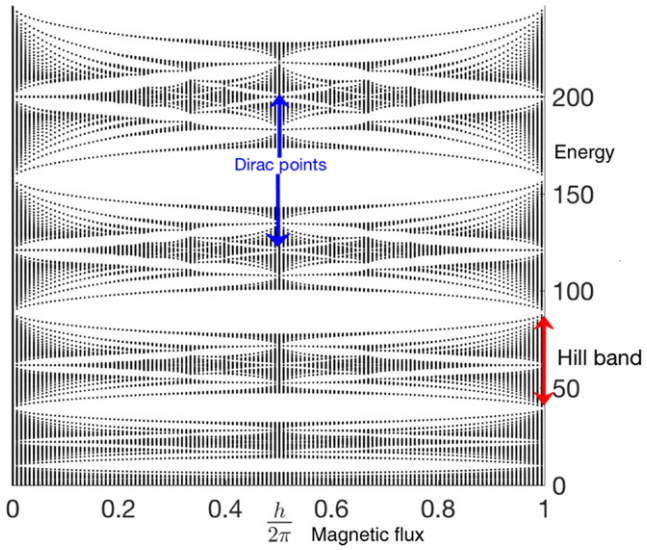

Figure 2. Hofstadter butterfly on honeycomb lattice. The spectrum of the quantum graph Hamiltonian H^B, (1), is plotted as a function of the magnetic flux $h \in [0, 2\pi]$. The blue arrows point at the location of the Dirac cones that are preserved at a fixed energy level. The Hill band is here the name of a single band of the non-magnetic Schrödinger operator and the spectrum of the magnetic Schrödinger operator is always contained in a Hill band. Reproduced from [49]. CC BY 4.0.

for some reduced fraction, we have the estimate

$$|\mathrm{Spec}(t^h)| \leqslant Cq^{-1/2}. \tag{5}$$

Here, $|A|$ denotes the Lebesgue measure of a set A. In other words, in the limit $q \to \infty$ the measure of the spectrum will tend to zero. In order to make this limit rigorous, we use that the spectrum of the tight-binding operator (2) is continuous (in Hausdorff distance d_{H}) with respect to the magnetic flux [49, lemma 6.2], i.e. there is a constant $C > 0$ such that

$$d_{\mathrm{H}}\left(\mathrm{Spec}\left(t^h\right), \mathrm{Spec}\left(t^{h'}\right)\right) \leqslant C|h - h'|^{1/4}. \tag{6}$$

To summarize, if $\frac{h}{2\pi}$ is irrational, the spectrum of (2), and the continuous spectrum of (1), is a fully disconnected and nowhere dense set without isolated points of measure zero. For irrational fluxes $\frac{h}{2\pi}$ with unbounded continued fraction expansion, the Lebesgue measure of the spectrum vanishes by combining estimate (5) and the continuity estimate (6). Since the spectrum is always closed and, as can be shown, it has no isolated points which would always imply point-spectrum, this implies Cantor-type spectrum. Using Kotani's theory, [65], the Cantor structure of the spectrum can also be shown to hold for all irrational fluxes $\frac{h}{2\pi}$.

After establishing the Cantor nature of the spectrum, it is reasonable to ask the question what the Hausdorff dimension of the spectrum is. We find that for irrational magnetic flux, the Hausdorff dimension is at most $\frac{1}{2}$ [50, theorem 1.5]. This bound on the Hausdorff dimensions follows from an almost Lipschitz continuity estimate on the spectrum of singular quasiperiodic Jacobi operators obtained in [50] and solves half of a conjecture by Wilkinson and Austin [44].

2. Semiclassical analysis of the DOS

The DOS is a *generalized function* ρ_{H^B} defined in terms of the regularized trace for suitable functions f

$$\begin{aligned}\widetilde{\mathrm{tr}}(f(H^B)) &= \lim_{r\to\infty} \frac{\mathrm{tr}\mathbb{1}_{B_r(0)} f(H^B)}{|B_r(0)|} \\ &= \int_{\mathbb{R}} f(x)\rho_{H^B}(x)\mathrm{d}x\end{aligned},$$

where $B_r(0)$ is the ball of radius r, see figures 3 and 4. Our method to analyse the DOS starts from the Helffer–Sjöstrand formula, [38], which states that for any Hamiltonian H and suitable functions f

$$f(H) = \frac{1}{\pi}\int_{\mathbb{C}} \partial_{\bar z}\widetilde{f}(H-z)^{-1}\mathrm{d}z,$$

where $\widetilde{f}$ is a smooth extension of f to the complex plane that satisfies the important feature that $\partial_{\bar z}\widetilde{f}(z)$ vanishes up to infinite order on the real line. Due to the last property, this function is also called an *almost analytic extension* of f. By spectral equivalence of (1) and (2), for energies close to the Dirac point energy it suffices to analyse the DOS of t^h. To define the DOS for the discrete operator t^h, we introduce a regularized trace for discrete operators A with $\mathbb{C}^2$-valued kernel $(A(x,y))$, by

$$\widehat{\mathrm{tr}}\, A := \lim_{r\to\infty} \frac{1}{|B_r(0)|} \sum_{\gamma\in\Lambda\cap B_r(0)} \mathrm{tr}_{\mathbb{C}^2} A(\gamma,\gamma). \tag{7}$$

Our method of analyzing the DOS of the tight-binding operator t^h, however, uses an equivalent representation of this operator as a differential operator which goes as follows: the magnetic translations in (2) satisfy the Weyl commutation relations

$$\tau^1\tau^0 = \mathrm{e}^{\mathrm{i}h}\,\tau^0\tau^1$$

and the same commutation relation holds for $D_x := -i\frac{\partial}{\partial x}$ by

$$\mathrm{e}^{\mathrm{i}hD_x}\,\mathrm{e}^{\mathrm{i}x} = \mathrm{e}^{\mathrm{i}h}\,\mathrm{e}^{\mathrm{i}x}\,\mathrm{e}^{\mathrm{i}hD_x}.$$

This different representation reduces the analysis of the DOS of (1) to the study of the DOS of the operator

$$\frac{1}{3}\begin{pmatrix} 0 & 1+\mathrm{e}^{\mathrm{i}x}+\mathrm{e}^{\mathrm{i}hD_x} \\ 1+\mathrm{e}^{-\mathrm{i}x}+\mathrm{e}^{-\mathrm{i}hD_x} & 0\end{pmatrix}. \tag{8}$$

We shall now use phase space variables (x,ξ) where the quantization of ξ is hD_x. Through a symplectic change of variables,

$$y = a(x+\xi), \eta = b\left(\xi - x \pm \frac{4\pi}{3}\right),$$

where $(a = \pm 2^{-\frac{1}{2}}3^{-\frac{1}{4}}, b = \pm 2^{-\frac{1}{2}}3^{\frac{1}{4}})$ one finds that at the Dirac points we have

$$\begin{aligned}1+\mathrm{e}^{\mathrm{i}x}+\mathrm{e}^{\mathrm{i}\xi} &= c(\eta \mp iy) + \mathcal{O}(y^2+\eta^2), \\ 1+\mathrm{e}^{-\mathrm{i}x}+\mathrm{e}^{-\mathrm{i}\xi} &= c(\eta \pm iy) + \mathcal{O}(y^2+\eta^2),\end{aligned} \tag{9}$$

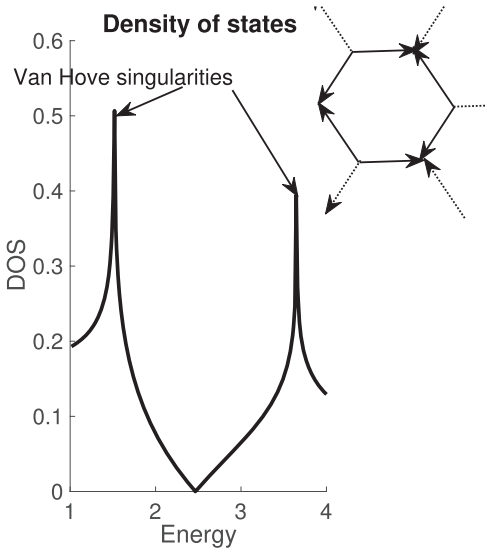

Figure 3. The DOS of the quantum graph model without magnetic of field obtained using $H^{B=0}$ (1) and $V = 0$ on the first band $[0, \pi^2]$. The comparison of the DOS of the quantum graph Hamiltonian H^B in (1) shows a striking agreement with the experimentally measured DOS in molecular graphene [17, figure 1].

$c = 3^{\frac{1}{4}}2^{-\frac{1}{2}}$. Classical-quantum correspondence implies that by the symplectic change of variables (*classical*), operator (8) is (micro)-locally equivalent (*quantum*) to the operator

$$\frac{c}{3}\begin{pmatrix} 0 & a_{\pm}^{*} \\ a_{\pm} & 0 \end{pmatrix}$$

quantized in new variables $a_{\pm} := y \pm ihD_y$. The spectrum of this operator can be explicitly expressed through the quantum harmonic oscillator. By making these steps precise and taking higher order contributions of the geometry, that are not captured by the Taylor expansion in (9) into account, it is possible to show the semiclassical Bohr–Sommerfeld description of the DOS with precise error control [10, theorem 1]: if $I \subset \Delta^{-1}(-\delta, \delta)$ is a small energy window around the Dirac points, with $\delta > 0$ small, then the DOS admits an expansion

$$\begin{aligned} &\widetilde{\mathrm{tr}}\, f(H^B) = \frac{2h}{3\sqrt{3}\pi}\sum_{n\in\mathbb{Z}^2} f(z_n(h)) + \mathcal{O}(|f|_{C^\alpha} h^\infty) \\ &\Delta(z_n(h)) = \kappa(nh, h). \quad \alpha > 0. \end{aligned} \tag{10}$$

The notation $\mathcal{O}(|f|_\alpha h^\infty)$ means here that for any N there is a constant $C_N > 0$ such that

$$\left| \widetilde{\mathrm{tr}}\, f(H^B) - \frac{2h}{3\sqrt{3}\pi}\sum_{n\in\mathbb{Z}^2} f(z_n(h)) \right| \leqslant C_N |f|_\alpha h^N,$$

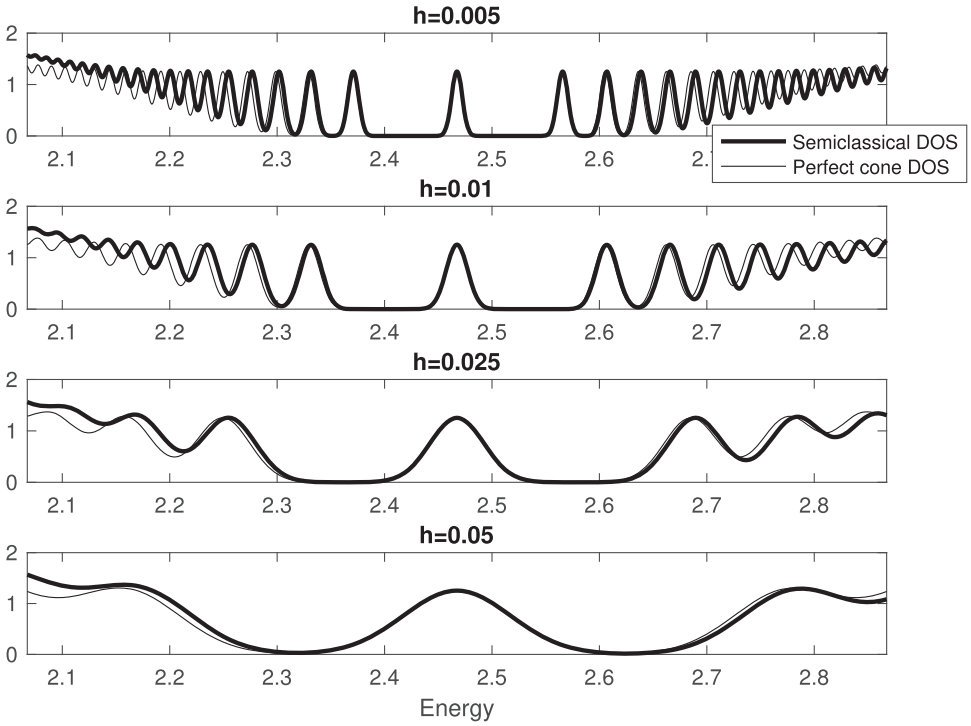

Figure 4. *Shubnikov–de Haas oscillations* of $\mu \mapsto \rho_{H^B}(\exp((\bullet-\mu)^2/2\sigma^2)/\sqrt{2\pi}\sigma)$ for different values of h. We note the asymmetry when compared to the DOS assuming perfect cones, i.e. the particle–hole symmetry. Reprinted by permission from Springer Nature Customer Service Centre GmbH: Springer Nature, Communications in Mathematical Physics, [10], Copyright (2019).

where $|f|_{C^\alpha} := \sup_x |f(x)| + \sup_{x\neq y} \frac{|f(x)-f(y)|}{|x-y|^\alpha}$. The quantities $\kappa(nh,h)$ appearing in (10) are the solutions to the Bohr–Sommerfeld condition

$$F(\kappa(\zeta,h)^2,h) = |\zeta| + \mathcal{O}(h^\infty),$$

where the function F possesses an expansion

$$\begin{aligned} F(s,h) &\sim F_0(s) + \sum_{j=2}^{\infty} h^j F_j(s), \quad F_0(s) = \frac{1}{4\pi}\int_{\gamma_s} \xi \,\mathrm{d}x, \\ \gamma_s &= \left\{(x,\xi)\in\mathbb{T}^2_* : \frac{|1+\mathrm{e}^{\mathrm{i}x}+\mathrm{e}^{\mathrm{i}\xi}|^2}{9} = s\right\}, \quad F_j(0) = 0. \end{aligned} \tag{11}$$

The leading order contribution F_0 here is therefore just the usual integral over the level-set in phase space. In particular, we show that the next-to leading order term, F_1, always vanishes, i.e. $F_1(s) = 0$ for all such 2×2 operators with only off-diagonal contributions, as for example (2). Writing $g(x) = F_0(\Delta(x)^2)$, we obtain a leading order approximation of Landau levels

$$z^{(1)}_{\pm|n|}(h) = g^{-1}_{\pm}(|n|h), \qquad z^{(1)}_0(h) = 0. \tag{12}$$

In (10), it is essential to allow non-smooth test functions f in view of applications to magnetic oscillations. Compare also with [1] for a different perspective on semiclassical approximations in this setting.

Figure 4 shows that Landau levels, and thus the DOS are non-symmetric with respect to the Dirac point energy. We compare this with the symmetric leading order (*perfect cone*) approximation of phase space area $g_c(x) = (x - z_D)^2/v_F^2$ with Fermi velocity

$$v_F = 3^{-3/4}\Delta'(z_D)^{-1}$$

and Dirac point energy $z_D \in \Delta^{-1}(0)$. Our expansion of the DOS in (10) is also essential for the understanding of *de-Haas van Alphen oscillations*. To formulate it we introduce the *grand-canonical potential* with inverse temperature β and chemical potential μ:

$$\begin{aligned} &\Omega_\beta(\mu, h) := \rho_B(\eta(\bullet) f_\beta(\mu - \bullet)) = \widetilde{\mathrm{tr}}(\eta(H^B) f_\beta(\mu - H^B)), \\ &f_\beta(x) := -\beta^{-1} \log(e^{\beta x} + 1) \simeq -x_+, \quad \beta \to +\infty, \end{aligned} \tag{13}$$

for smooth η localizing to energy intervals contained in $\Delta^{-1}(-\delta, \delta)$. (Note that $|f_\beta|_\alpha$ is uniformly bounded for $\alpha \leqslant 1$ but not for $\alpha > 1$.) For the study of these oscillations, recall that the *magnetization* is defined by [3]

$$M_\beta(\mu, h) := -\frac{3\sqrt{3}}{2}\frac{\partial}{\partial h}\Omega_\beta(\mu, h) \tag{14}$$

and at zero temperature, we can derive from this a *sawtooth approximation*, with $\sigma(y) := y - [y] - \frac{1}{2}$, as the $\mathcal{O}(h^{\frac{1}{2}})$ approximation of (14) shows

$$M_\infty(\mu, h) = \frac{1}{\pi}\sigma\left(\frac{g(\mu)}{h}\right)\frac{g(\mu)}{g'(\mu)} + \mathcal{O}\left(h^{\frac{1}{2}}\right). \tag{15}$$

This provides a refinement of results found in [2, 4, 5]. The remarkable agreement of the different expressions for the magnetization is illustrated in figure 5: the characteristic sawtooth pattern (15) is compared with the magnetization computed from (14), using either the operator spectrum or the semiclassical limit (10).

3. QHE, Dirac points, and self-similarity

One of the striking properties of graphene is the existence of Dirac points, which has remarkable physical and technological implications [66]. It turns out Dirac points persist in the tight-binding Hamiltonian (2) at energy $E = 0$ for any rational magnetic flux $h_0 = 2\pi p/q$, [51, theorem 2], yet the opening angle is highly dependent on the flux. This persistence and dependence of the opening angle on the flux then causes (part of) the self-similarity in the Hofstadter butterfly on the honeycomb lattice.

To explain this phenomenon, let us recall that for rational magnetic flux, Floquet theory allows us to express the tight-binding Hamiltonian in terms of a matrix

$$M(k) = \frac{1}{3}\begin{pmatrix} 0 & I_q + \mathrm{e}^{\mathrm{i}k_1} J_{p,q} + \mathrm{e}^{\mathrm{i}k_2} K_q \\ \text{h.c.} & 0 \end{pmatrix},$$

where $J_{p,q}$ and K_q are $q \times q$ matrices, defined as

$$J_{p,q} = \mathrm{diag}(\{\mathrm{e}^{\mathrm{i}(j-1)h_0}\}_{j=1}^{q}),$$

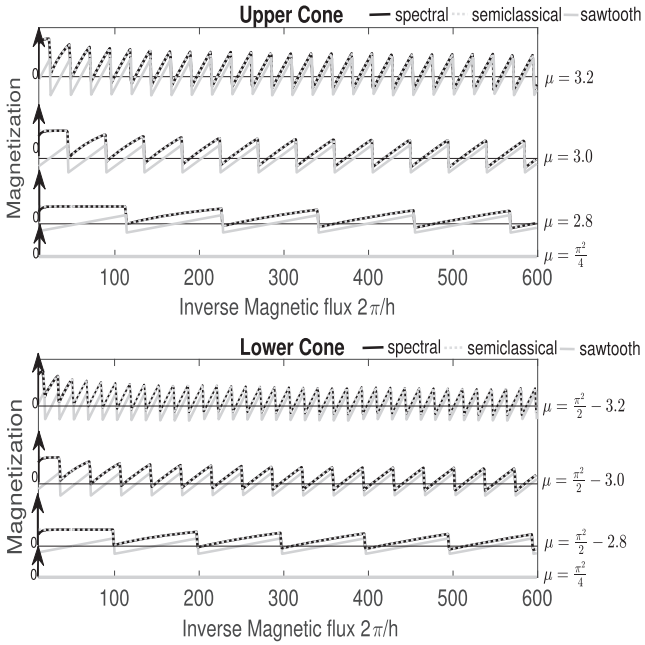

Figure 5. Magnetization (14) for the quantum graph Hamiltonian (1) for different chemical potentials *above/below* the Dirac energy $\mu = \frac{\pi^2}{4}$, with $V \equiv 0$. We observe the asymmetry between the oscillations on the upper and lower cone. Reprinted by permission from Springer Nature Customer Service Centre GmbH: Springer Nature, Communications in Mathematical Physics, [10], Copyright (2019).

and

$$(K_q)_{jk} = \begin{cases} 1 & \text{if } k \equiv j+1 (\mathrm{mod}\, q) \\ 0 & \text{otherwise.} \end{cases}.$$

By squaring the matrix $M(k)$, we find a diagonal matrix

$$M(k)^2 = \frac{1}{9}\begin{pmatrix} 3I_q + M_{\mathrm{T}}(k) & 0 \\ 0 & 3I_q + \hat{M}_{\mathrm{T}}(k) \end{pmatrix},$$

with

$$\begin{aligned} \hat{M}_{\mathrm{T}}(k) = {} & \mathrm{e}^{\mathrm{i}k_1} J_{p,q} + \mathrm{e}^{-\mathrm{i}k_1} J_{p,q}^{\dagger} + \mathrm{e}^{\mathrm{i}k_2} K_q + \mathrm{e}^{-\mathrm{i}k_2} K_q^{\dagger} \\ & + \mathrm{e}^{\mathrm{i}(k_1-k_2)} K_q^{\dagger} J_{p,q} + \mathrm{e}^{-\mathrm{i}(k_1-k_2)} J_{p,q}^{\dagger} K_q, \end{aligned} \tag{16}$$

and for $M_{\mathrm{T}}(k)$ one just exchanges $J_{p,q}$ and K_q.

One then has a chambers-type formula [68] for the characteristic polynomial of $M_{\mathrm{T}}(k)$

$$\begin{aligned} \det(M_{\mathrm{T}}(k) - \lambda) = {} & f_{p,q}(\lambda) + 2(-1)^{q+1} \\ & \times (\cos qk_1 + \cos qk_2 + (-1)^{q+1} \cos q(k_1 - k_2)), \end{aligned} \tag{17}$$

where $f_{p,q}$ is a polynomial in λ that does not depend on k. The advantage of this expansion for the determinant is that the dependence on the quasi-momentum k is made fully explicit. In particular, we see that zero eigenvalues of $M(k)$, or eigenvalues -3 of M_{T} are located at quasi-momenta

$$k = \left(\frac{\pi}{3q}, -\frac{\pi}{3q}\right) \text{for even } q, \text{and } k = \left(\frac{2\pi}{3q}, -\frac{2\pi}{3q}\right) \text{for odd } q.$$

Taylor expanding the expression (17) at the quasi-momenta at which the Dirac cones are situated then yields the following expansion of the DOS, similar to (10) for a magnetic flux $h = h_0 + \varepsilon$ with ε small

$$\begin{aligned} &\widehat{\mathrm{tr}}\, f(t^B) = \frac{2q\varepsilon}{3\sqrt{3}\pi} \sum_{n\in\mathbb{Z}^2} f(z_n(\varepsilon)) + \mathcal{O}(|f|_{C^\alpha}\varepsilon^\infty) \\ &\text{where } z_n(\varepsilon) = v_{\mathrm{F}}\ \mathrm{sgn}(n)\sqrt{|n\varepsilon|} + \mathcal{O}(\varepsilon). \end{aligned} \tag{18}$$

Here, the Fermi velocity is explicitly given by

$$v_{\mathrm{F}} = 3^{3/4} q \left(3^{q-1} \prod_{j=q+2}^{2q} \tilde{t_j^{h_0}}(k)\right)^{-1},$$

where $\tilde{t_j^{h_0}}(k)$ is the jth Floquet eigenvalue to t^{h_0}, increasingly ordered, with quasi-momentum $\widetilde{k}$ where B_0 is the magnetic field associated to the flux $h_0 = \frac{2\pi p}{q}$. This study is inherently connected with self-similarity in the Hofstadter butterfly, see the plot of the coloured Hofstadter butterfly in figure 6, and also with the occurrence of magnetic mini-bands [8]. To link this analysis to the quantum Hall effect, we recall since the tight-binding Hamiltonian t^h is an element of the rotation algebra, so is its Fermi projection $P = \mathbb{1}_{[z_{\mathrm{D}},\mu)}(t^h)$ for Fermi energies μ inside a spectral gap of t^h. By [69–71], there is $\gamma \in \mathbb{Z}^2$, such that for

$$\widehat{\mathrm{tr}}(P) = \frac{2}{3\sqrt{3}}(\gamma_1 + \gamma_2 \frac{\varepsilon}{2\pi}), \tag{19}$$

where by comparing this expression with (18), we see that $\gamma = (0, 2qn)$ and n is the number of Landau levels between z_{D} and μ. Combining (18) with (5) implies the existence of spectral gaps between a finite number of disjoint intervals $\mathcal{B}_n(\varepsilon) \ni z_n(\varepsilon)$ up to some small disorder strength $\kappa_0 > 0$. The Hall conductivity, which by universality (see [72, 73]) is invariant under weak disorder, is given by Středa's formula [74] as

$$c_{\mathrm{H}}(\mu) := \frac{\partial}{\partial\varepsilon}\, \widehat{\mathrm{tr}}(\mathbb{1}_{[z_{\mathrm{D}},\mu)}(t^h_{\kappa,\omega})) = \frac{\gamma_2}{2\pi}$$

with Fermi energies μ in the interval I_n between $B_n(\varepsilon)$ and $B_{n+1}(\varepsilon)$ [51, proposition 1.1 & theorem 4]. From (18) and (19) we then find

$$c_{\mathrm{H}}(\mu) = \begin{cases} \dfrac{(2n+1)q}{2\pi}, & \mu \in I_n,\ n \geqslant 0 \\ \dfrac{(2n-1)q}{2\pi}, & \mu \in I_{n-1},\ n \leqslant 0. \end{cases} \tag{20}$$

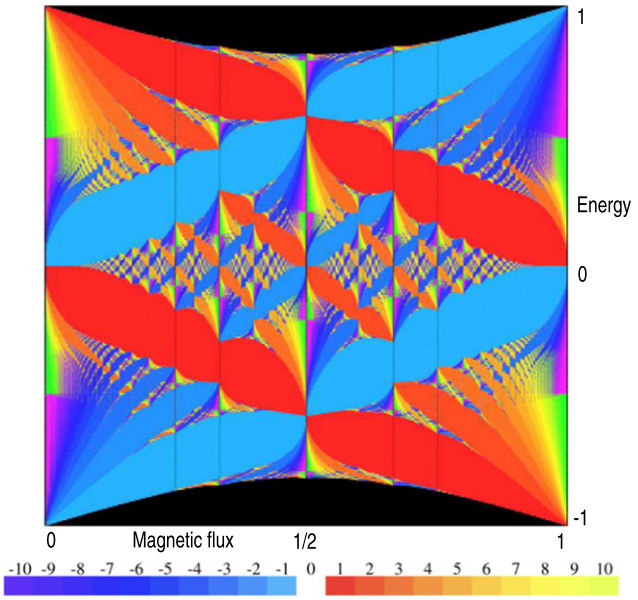

Figure 6. Coloured Hofstadter butterfly on honeycomb lattice for tight-binding Hamiltonian (2) for all possible magnetic fluxes $\frac{h}{2\pi}$. Different colours correspond to different Hall conductivities as indicated in the colourbar.

This expression is only valid for Fermi energies close to the conical point. The Hall conductivity for arbitrary Fermi energies is far more intricate, as illustrated in the coloured Hofstadter butterfly in figure 6 that covers the entire spectrum of (2), cf [67, 75].

4. Metal/insulator transition

To study transport properties on honeycomb structure (see [67, 76–78]) we consider the tight-binding operator (2) with additional additive disorder

$$t^h_{\kappa,\omega} = \frac{1}{3}\begin{pmatrix} -\kappa V^{(1)}_{\omega} & 1+\tau^0+\tau^1 \\ (1+\tau^0+\tau^1)^\dagger & -\kappa V^{(2)}_{\omega} \end{pmatrix}, \tag{21}$$

where $(V^{1,2}_{\omega(z)})_{z\in\mathbb{Z}^2}$ are independent and identically distributed random variables with compactly supported probability distribution and small $\kappa > 0$.

The Hall conductivity allows us also to analyse transport properties of $t^h_{\kappa,\omega}$. Transport in disordered media at energy E is measured by transport coefficients $\beta^h_\kappa(E)$ [48, 79–82]. This quantity allows us to define two complementary energy regions, the *insulator region*

$$\Sigma^{h,\mathrm{DL}}_\kappa = \left\{E \in \mathbb{R}; \beta^h_\kappa(E) = 0\right\}$$

and the *metallic transport region*

$$\Sigma^{h,\mathrm{DD}}_\kappa = \left\{E \in \mathbb{R}; \beta^h_\kappa(E) > 0\right\}.$$

Energies $E \in \Sigma^{h,\mathrm{DD}}_\kappa$ at which the transport coefficient β^h_κ jumps from zero to a non-zero value are called *mobility edges*, while energies $E \in \Sigma^{h,\mathrm{DL}}_\kappa(H^h_{\kappa,\omega})$, that also belong to the spectrum of

(21), are eigenvalues of finite multiplicity with exponentially decaying eigenfunctions (*Anderson localization*). From the jumps of the Hall conductivity, we conclude [51, theorem 1] that there exist mobility edges E close to each Landau level with non-trivial transport $\beta^h_\lambda(E) \geqslant 1/4$. In contrast to this, it is easy to see, by verifying the starting criteria of the multi-scale analysis [47, 51, 80] that the spectral gaps between the Landau levels can only be filled with spectrum belonging to the insulating region [51, proposition 5.5] in which the operator (21) therefore exhibits Anderson localization.

5. Conclusion and open questions

In this article, we obtain a number of new results and rigorous refinements for the tight-binding model as well as the quantum graph model on the honeycomb lattice in a constant magnetic field. Our findings can be divided into three subparts.

The first part is concerned with the nature of the spectrum. While it is a classical result based on Floquet theory that for rational magnetic flux $\frac{h}{2\pi}$ the spectrum of the tight-binding Hamiltonian has band structure. The situation changes quite dramatically for irrational $\frac{h}{2\pi}$. In this case, we show the spectrum becomes a Cantor set of Lebesgue measure zero. In addition, we show one part of a conjecture by Thouless which is that the Hausdorff dimension of the spectrum is at most $1/2$. The opposite direction remains largely open.

We then perform a semiclassical analysis of the DOS close to any rational number, taking into account asymmetries of the Dirac cones, obtain analytical expressions for the Fermi velocity, and apply our results to a study of magnetic oscillations, the quantum Hall effect, and self-similarity in the Hofstadter butterfly.

Finally, we discuss the case of additional disorder and obtain estimates on transport coefficients. Here, it would be desirable to obtain refined estimates on the estimates that contribute to the regime of transport.

Acknowledgments

SB gratefully acknowledges support by the UK Engineering and Physical Sciences Research Council (EPSRC) Grant EP/L016516/1 for the University of Cambridge Centre for Doctoral Training, the Cambridge Centre for Analysis. RH, SJ, and MZ were partially supported by the National Science Foundation under the Grants DMS-1800689, 1500852 and 1901462.

Data availability statement

All data that support the findings of this study are included within the article (and any supplementary files).

ORCID iDs

Becker Simon https://orcid.org/0000-0002-6703-9511

References

[1] Carmier P and Ullmo D 2008 *Phys. Rev.* B **77** 245413
[2] Sharapov S G, Gusynin V P and Beck H 2004 *Phys. Rev.* B **69** 075104

[3] Onsager L 1952 *Philos. Mag.* **7** 43
[4] Champelde T and Mineev V P 2001 *Philos. Mag.* **B81** 55–74
[5] Lukýanchuka A 2011 *Low Temp. Phys.* **37** 45
[6] Kostrykin V and Schrader R 2003 *Commun. Math. Phys.* **237** 161–79
[7] Rhim J-W and Park K 2012 *Phys. Rev.* B **86** 235411
[8] Chen X, Wallbank J, Patel A, Mucha-Kruczyski M, McCann E and Fal'ko V 2014 *Phys. Rev.* B **89** 075401
[9] Kishigi K and Hasegawa Y 2014 *Phys. Rev.* B **90** 085427
[10] Becker S and Zworski M 2019 *Commun. Math. Phys.* **367** 941–89
[11] Stauber T, Parida P, Trushin M, Ulybyshev M V, Boyda D L and Schliemann J 2017 *Phys. Rev. Lett.* **118** 266801
[12] Küppersbusch C and Fritz L 2017 *Phys. Rev.* B **96** 205410
[13] Shoenberg D 1984 *Magnetic Oscillations in Metals* (Cambridge: Cambridge University Press)
[14] Heße L and Richter K 2014 *Phys. Rev.* B **90** 205424
[15] Gusynin V P and Sharapov S G 2005 *Phys. Rev.* B **71** 125124
[16] Tan Z, Tan C, Ma L, Liu G T, Lu L and Yang C L 2011 *Phys. Rev.* B **84** 115429
[17] Gomes K K, Mar W, Ko W, Guinea F and Manoharan H C 2012 *Nature* **483** 306–10
[18] Reich S, Maultzsch J, Thomsen C and Ordejón P 2002 *Phys. Rev.* B **66** 035412
[19] Dietz B, Klaus T, Miski-Oglu M and Richter A 2015 *Phys. Rev.* B **91** 035411
[20] Das A, Kaul R K and Murthy G 2020 *Phys. Rev.* B **101** 165416
[21] Lavor I R, da Costa D R, Chaves A, Farias G A, Macêdo R and Peeters F M 2020 *J. Phys.: Condens. Matter.* **32** 155501
[22] Azbel M 1964 *Sov. Phys. JETP* **19** 634–45
[23] Hofstadter D R 1976 *Phys. Rev.* B **14** 2239–49
[24] Garcia-Cervantes H, Gaggero-Sager L, Díaz-Guerrero D S, Sotolongo-Costa O and Rodríguez-Vargas I 2017 *Sc. Reports* **7** 1
[25] Ponomarenko L A *et al* 2013 *Nature* **497** 594–7
[26] Kuhl U and Stöckmann H-J 1998 *Phys. Rev. Lett.* **80** 3232–5
[27] Bellissard J and Simon B 1982 *J. Funct. Anal.* **48** 408–19
[28] Avron J, van Mouche P H M and Simon B 1990 *Commun. Math. Phys.* **132** 103–18
[29] Last Y 1994 *Commun. Math. Phys.* **164** 421–32
[30] Jitomirskaya S Y and Last Y 1998 *Commun. Math. Phys.* **195** 1–14
[31] Jitomirskaya S Y and Krasovsky I V 2002 *Math. Res. Lett.* **9** 413–21
[32] Ávila A and Krikorian R 2006 *Ann. Math.* **164** 911–40
[33] Avila A and Jitomirskaya S 2005 *Lecture Notes in Physics* vol 690 (Berlin: Springer) pp 5–16
[34] Jitomirskaya S and Zhang S 2015 arXiv:1510.07086
[35] Last Y and Shamis M 2016 *Commun. Math. Phys.* **348** 729–50
[36] Helffer B, Liu Q, Qu Y and Zhou Q 2019 *Commun. Math. Phys.* **368** 369–82
[37] Helffer B and Sjöstrand J 1989 *Mém. Soc. Math. France* **34** 1–124
[38] Helffer B and Sjöstrand J 1989 *Schrödinger Operators* (*Lecture Notes in Physics* vol 345) (Berlin: Springer) pp 118–97 (Sønderborg, 1988)
[39] Helffer B and Sjöstrand J 1990 *Mém. Soc. Math. France* **40** 1–139
[40] Helffer B and Sjöstrand J 1990 On diamagnetism and de Haas–van Alphen effect *Ann. Inst. Henri Poincaré Phys. Théor.* **52** 303–75
[41] Ketzmerick R, Kruse K, Steinbach F and Geisel T 1998 *Phys. Rev.* B **58** 1103
[42] Geisel T, Ketzmerick R and Petshel G 1991 *Phys. Rev. Lett.* **66** 3321
[43] Tang C and Kohmoto M 1986 *Phys. Rev.* B **34** 2041(R)
[44] Wilkinson M and Austin E J 1990 *J. Phys. A: Math. Gen.* **23** 2529–53
[45] Anderson P W 1958 *Phys. Rev.* **109** 1492–505
[46] Sato M, Tobe D and Kohmoto M 2008 Hall conductance, topological quantum phase transition, and the diophantine equation on the honeycomb lattice *Phys. Rev.* B **78** 235322
[47] Fröhlich J and Spencer T 1983 *Commun. Math. Phys.* **88** 151–84
[48] Germinet F, Klein A and Schenker J 2007 *Ann. Math.* **166** 215–44
[49] Becker S, Han R and Jitomirskaya S 2019 *Invent. math.* **218** 979–1041
[50] Jitomirskaya S and Krasovsky I 2019 arXiv:1909.04429
[51] Becker S and Han R 2021 *Int. Math. Res. Not.* rnab017
[52] Kuchment P and Post O 2007 *Commun. Math. Phys.* **275** 805–26
[53] Helffer B, Kerdelhué P and Royo-Letelier J 2016 *Ann. Henri Poincaré* **17** 795–818

[54] Drouot A 2019 *Commun. PDE* **44** 1406–30
[55] Drouot A, Fefferman C and Weinstein M 2018 arXiv:1810.05875
[56] Fefferman C L and Weinstein M I 2012 *J. Am. Math. Soc.* **25** 1169–220
[57] Fefferman C, Lee-Thorp J and Weinstein M 2016 *Commun. Pure Appl. Math.* **71** 1178–270
[58] Avila A and Jitomirskaya S 2009 *Ann. Math.* **170** 303–42
[59] Brüning J, Geyler V and Pankrashkin K 2007 *Commun. Math. Phys.* **269** 87–105
[60] Polini M, Guinea F, Lewenstein M, Manoharan H C and Pellegrini V 2013 *Nat. Nanotechnol.* **8** 625–33
[61] Pankrashkin K 2006 *Lett. Math. Phys.* **77** 139–54
[62] Pankrashkin K 2013 *J. Funct. Anal.* **265** 2910–36
Pankrashkin K 2013 *J. Funct. Anal.* **265** 640–55
[63] Pankrashkin K 2012 *J. Math. Anal. Appl.* **396** 640–55
[64] Bena C and Montambaux G 2009 *New J. Phys.* **11** 095003
[65] Teschl G 2000 *Mathematical Surveys and Monographs* vol 72 (Providence, RI: American Mathematical Society)
[66] Wong H-S P and Akinwande D 2010 *Carbon Nanotube and Graphene Device Physics* (Cambridge: Cambridge University Press)
[67] Agazzi A, Eckmann J-P and Graf G-M 2014 *J. Stat. Phys.* **156** 417–26
[68] Helffer B, Kerdelhué P and Royo-Letelier J 2016 Chambers's formula for the graphene and the Hou model with Kagome periodicity and applications *Ann. Henri Poincaré* **17** 795–818
[69] Pimsner M and Voiculescu D 1980 *J. Operat. Theory* 93–118
[70] Pimsner M and Voiculescu D 1980 *J. Operat. Theory* 201–10
[71] Rieffel M 1981 *Pacific J. Math.* **93** 415–29
[72] Avron J E, Seiler R and Simon B 1994 *Commun. Math. Phys.* **159** 399–422
[73] Bellissard J, van Elst A and Schulz- Baldes H 1994 *J. Math. Phys.* **35** 5373–451
[74] Streda P 1982 *J. Phys. C: Solid State Phys.* **15** L717
[75] Zhang Y, Tan Y-W, Stormer H L and Kim P 2005 *Nature* **438** 201–4
[76] Gusynin V P and Sharapov S G 2006 *Phys. Rev.* B **73** 245411
[77] Morozov S V, Novoselov K S, Katsnelson M I, Schedin F, Ponomarenko L A, Jiang D and Geim A K 2006 *Phys. Rev. Lett.* **97** 016801
[78] Peres N 2010 *Rev. of Mod. Phys.* **82** 2673
[79] Germinet F and Klein A 2001 *Commun. Math. Phys.* **222** 415–48
[80] Germinet F and Klein A 2003 *Geom. Funct. Anal.* **13** 1201–38
[81] Germinet F and Klein A 2004 *Duke Math. J.* **124** 309–50
[82] Germinet F and Klein A 2006 *J. Stat. Phys.* **122** 73–94